What generates daily cycles of marine snow?

JAVIER RUIZ*

Abstract—The recent discovery of daily cycles in the concentration of marine aggregates raises questions regarding the process producing the cycles and whether or not aggregation theory is able to predict them. A model of particle dynamics was used to study these questions. The model incorporated particle aggregation, break-up and sedimentation as well as diel growth and grazing. Three main processes considered to be possible causes for daily cycles of marine aggregates (growth, turbulence and grazing) were tested with the model. The results demonstrated that aggregation theory is able to predict daily cycles of marine aggregates. Neither the daily cycle of growth, nor that of grazing, was able to generate daily cycles alone. However, daily cycles of marine turbulence in the mixed layer caused a clear cyclic behaviour of particulate matter in the model. Therefore, these results suggested that diel variation of turbulence is the best candidate to explain the daily cycles of aggregates observed in the sea. © 1997 Elsevier Science Ltd

NOTATION

a	Gravitational acceleration (980 cm s^{-2}).
$a_L^{\#}$	Spectrally averaged photosynthetic parameter of Anderson (1993) model.
b_1, b_2	Constants of the Dobson and Smith (1988) model.
b_3, b_4	Parameters of the particle size distribution function.
b_5, b_6	Constants of the Jackson (1995) break-up model.
$B_{(agg < 0.02\ cm)}$	Nitrogen concentration of aggregates smaller than 0.02 cm (μM).
c	Chlorophyll concentration (mg chlorophyll m^{-3}).
C	Relaxation factor for the hydrodynamic impedance to particle contact (Hill, 1992).
d	Aggregate diameter.
d_k	Nominal diameter (cm) of aggregates in size class k.
E_{ij}	Probability of contact between particles when in proximity.
$f(R)$	Function to switch on and off zooplankton grazing.
g	Growth rate of phytoplankton (s^{-1}).
g_r	Maximum specific grazing rate (1.16×10^{-5} s^{-1}).
G_k	Grazing rate on size class k (μM s^{-1}).
H	User-defined parameter in the Ruiz and Izquierdo (in press) model.
I_o	Photosynthetically active radiation just beneath the ocean surface (μE m^{-2} s^{-1}).
I_{L1}, I_{L2}	Light entering and leaving layer L (μE m^{-2} s^{-1}).
$J(\eta, x)$	Function in the Ruiz and Izquierdo (in press) model.
K	Half saturation constant for grazing (1 μM).
k_L	Spectrally averaged attenuation coefficient of layer L (m^{-1}).
$K_{ij(sedim)}$	Aggregation kernel for sedimentation (cm^3 s^{-1}).
$K_{ij(shear)}$	Aggregation kernel for shear (cm^3 s^{-1}).
K_{ij}	Total aggregation kernel (cm^3 s^{-1}).
$L(\eta)$	Nitrogen content of an aggregate of diameter η.

---

* Departamento de Biología y Ecología, Facultad de Ciencias del Mar, Universidad de Cádiz, Apartado núm. 40, 11510 Puerto Real, Cádiz, Spain.

$l(\eta, x)$	Function in the Ruiz and Izquierdo (in press) model.
$m(d)$	Nitrogen content of an aggregate of diameter d (μmoles N).
m_k	Nominal mass (μmoles) of aggregates in size class k.
M	Mixed layer depth (40 m).
n	Number of sublayers in mixed layer for phytoplankton growth model (3).
N_k	Number concentration (cm^{-3}) of aggregates in size class k.
No	Dissolved nitrogen concentration (μM).
$N(m, t)$	Particle size distribution function (μmoles of N)$^{-1}$.
p	d_i/d_j (i < j).
P	Porosity.
P_m^B	Assimilation number (6.04 mg C (mg chlorophyll)$^{-1}$ h^{-1}).
Q_k	Nitrogen concentration (μM) of aggregates in size class k.
R	Photosynthetically active radiation at the top of the atmosphere (μE m^{-2} s^{-1}).
r_k	Decay rate, by break-up, of particles in size class k (s^{-1}).
S	Sine of solar elevation.
T	Atmospheric transmission factor.
t_{ki}	Rate of production of k-particles by rupture of i-particles. (s^{-1}).
u_0, u_1, u_2, u_3	Depth limits of mixed layer sub-layers (m).
V_k	Nominal volume (cm^3) of aggregates in size class k.
w	Aggregate settling velocity (cm s^{-1}).
w_k	Nominal settling velocity (cm s^{-1}) of aggregates in size class k.
Y	Primary production integrated along the mixed layer (mg C m^{-2} h^{-1}).
Z	Zooplankton concentration (μM).
α	Probability that two aggregates stick after contact.
α_m^B	Maximum photosynthetic efficiency (0.026 mg C (mg chlorophyll)$^{-1}$ h^{-1} (μE m^{-2} s^{-1})$^{-1}$).
$\bar{\beta}$	Sectional aggregation kernel (μM^{-1} s^{-1}).
$\delta_{b1}, \delta_{b2}, \delta_{g1}, \delta_{g2}$	Conditional functions in Ruiz and Izquierdo (in press) model.
$\varepsilon(R)$	Rate of turbulent kinetic energy dissipation (cm^2 s^{-3}).
θ	Proportion of nitrogen in constituent matter (0.01).
μ	Sea water dynamic viscosity (0.01 gr cm^{-1} s^{-1}).
μ_z	Zooplankton mortality rate (5.8 $\times$ 10^{-7} s^{-1}).
ρ_c	Constituent matter density (gr cm^{-3}).
ρ_w	Sea water density (1.0217 gr cm^{-3}).
σ_z	Zooplankton assimilation efficiency.
υ	Sea water kinematic viscosity (0.01 cm^2 s^{-1}).

INTRODUCTION

Marine aggregates have recently received much attention because they are considered to play an important role in the export of organic matter to the ocean interior (Fowler and Knauer, 1986). Their importance lies in their high sinking velocities. Different studies on marine snow report their existence in a variety of marine environments including surface and deep waters, and coastal and open oceans (Alldredge and Silver, 1988). These studies have shown the presence of mid-depth maxima (Asper, 1987; Lampitt *et al.*, 1993b), higher concentrations in coastal than in oceanic waters (Alldredge, 1992) and high concentrations during phytoplankton blooms (Prézelin and Alldredge, 1983; Kranck and Milligan, 1988; Alldredge and Gotschalk, 1989).

However, some important aspects of marine snow dynamics have only recently become evident. Lampitt *et al.* (1993a) found a daily cycle in aggregate concentration at 270 m in the North Atlantic. The high temporal resolution (hours) of their time series permitted this discovery. They proposed that biological and physical processes in the upper water column or migrating zooplankton constitute the possible origin of these cycles. The upper water

column has diel cycles of phytoplankton production and turbulence levels caused by day–night differences in incoming radiation. Because of zooplankton migration it also has cycles of grazing mortality on phytoplankton populations. Any of these is, in principle, a good candidate for the origin of cycles in the concentration of marine snow aggregates.

The aim of this paper was to perform a modelling analysis of the three processes mentioned (zooplankton, production and turbulence) in order to see which is able to cause the daily cycles in marine aggregates. The results demonstrated that neither diel phytoplankton growth nor diel grazing alone are able to produce the observed cyclic behaviour of marine aggregates. However, daily cycles of mixed-layer turbulence produced a clear cyclic behaviour of particulate matter. Therefore, our results suggested that diel patterns in mixed-layer turbulence cause the observed daily changes in marine aggregate concentration and vertical flux.

MODEL

The equation governing the dynamics of particles in the mixed layer is:

$$\frac{dQ_k}{dt} = AGREGATION - BREAK\_UP + GROWTH - GRAZING - SEDIMENTATION \tag{1}$$

where Q_k is the mass concentration (μM of N) in the size class k. The interpretation and derivation of the different terms in equation (1) is explained below.

Aggregation

Several models for the aggregation of marine algal aggregates have been published since Jackson (1990) first implemented the physical aggregation of particles in a growing population of phytoplankton. The different models propose different formulations of the aggregation process. Owing to computational limitations, early models (Jackson, 1990; Riebesell and Wolf-Gladrow, 1992) were only able to study a small range of aggregate sizes. The equation used in these models has the form:

$$\frac{dN_k}{dt} = \frac{1}{2}\sum_{i+j=k} \alpha E_{ij} K_{ij} N_i N_j - N_k \sum_i \alpha E_{ik} K_{ik} N_i \tag{2}$$

where N_i is the number concentration of aggregates in the size class i, K_{ij} (the aggregation kernel with units of cm^3 s^{-1}) is a coefficient describing the frequency with which particles are brought into close proximity, E_{ij} is the probability that two particles make contact once they are in close proximity, and α is the probability that two aggregates remain stuck together after contact (Hill, 1992). Three different mechanisms dominate the bringing together of particles (McCave, 1984). The first is a result of the Brownian motion of particles. This mechanism is not included here as it is negligible for the size of particles considered in this model (McCave, 1984). The second mechanism is the differential sedimentation of particles. The resulting aggregation kernel is the difference in the settling velocity of the coagulating particles multiplied by the area of the circle resulting from the summation of the diameters of both particles (McCave, 1984).

$$K_{ij(sedim)} = \frac{\pi}{4}|w_i - w_j|(d_i + d_j)^2 \tag{3}$$

where w_i and w_j are the particle settling velocities and d_i and d_j are the particle diameters.

The third mechanism results from the relative motion between the suspended particles which is generated by turbulent shear. Different shear kernels have been proposed for particles larger or smaller than the Kolmogorov scale (Hill, 1992). Further investigations (Hill et al., 1992) demonstrated that the super-Kolmogorov formulation successfully predicted the relative velocity between particles that are one order of magnitude smaller than this scale. Therefore, two different expressions are used for the shear kernel. They correspond to the sub- and super-Kolmogorov kernels of Hill (1992) but the limit for implementing the super-Kolmogorov one is located at a smaller size than the Kolmogorov scale [equation (4)]. This is 0.01 cm because this is the size at which this formulation starts to be valid (Hill et al., 1992).

$$
\begin{aligned}
K_{ij(shear)}^{sub} &= 0.16(d_i + d_j)^3(\varepsilon(R)/v)^{1/2} &\quad \text{for } d_i, d_j < 0.01 \text{ cm} \\
K_{ij(shear)}^{sup} &= 1.08(d_i + d_j)^{7/3}(\varepsilon(R)^{1/3}) &\quad \text{for } d_i, d_j > 0.01 \text{ cm} \\
\varepsilon(R) &= 7\times10^{-8}\text{m}^2\text{s}^{-3} &\quad \text{for } R = 0 \\
\varepsilon(R) &= 10^{-9}\text{m}^2\text{s}^{-3} &\quad \text{for } R > 0
\end{aligned} \tag{4}
$$

where $\varepsilon(R)$ is the rate of turbulent kinetic energy dissipation, R is photosynthetically active radiation at the top of the atmosphere, d_i is the nominal diameter of size class i and v is the kinematic viscosity of sea water. The total aggregation kernel K_{ij} is the sum of the shear and differential sedimentation kernels. The values of turbulent energy dissipation alternated between low and high on a daily cycle. In the current model this was guided by radiation, which was calculated using the usual astronomical formulae (Brock, 1981). When it is positive $\varepsilon = 10^{-9}$ m^{2}s^{-3}, whereas for zero values of radiation $\varepsilon = 7 \times 10^{-8}$ m^{2}s^{-3}. These are around the average values recorded by Brainerd and Gregg (1993) for the diel changes of ε during an 11-day time series in the north-east Pacific.

E_{ij}, the probability that two particles make contact once they are in close proximity (Hill, 1992), is (Pruppacher and Klett, 1978):

$$E_{ij(sedim)} = \frac{p^2}{2(1 + p)^2} \tag{5}$$

for contact by differential sedimentation, where $p = d_i/d_j$ (i < j). Stolzenbach and Elimelech (1994) use the results of Wacholder and Sather (1974) to show that the rate of collision by differential sedimentation is zero for a wide size range of marine particles. However, it is not yet clear how this theory applies to porous particles (Stolzenbach and Elimelech, 1994).

For contact by shear the equation derived by Landau and Lifshitz (1959) was used:

$$E_{ij(shear)} = \frac{7.5p^2}{(1 + 2p)^2} \tag{6}$$

Hill (1992) noted the need to relax the hydrodynamic impedance to particle contact imposed by equations (5) and (6), which are valid for impermeable spheres. Marine aggregates are not impermeable spheres and higher contact rates than those predicted after

applying equations (5) and (6) must occur between them. Hill (1992) proposed to achieve this modification by redefining the parameter p as:

$$
\begin{aligned}
p &= C\frac{d_i}{d_j} \quad \text{for} \quad C\frac{d_i}{d_j} \leq 1 \\
p &= 1 \quad\quad \text{for} \quad C\frac{d_i}{d_j} > 1
\end{aligned}
\tag{7}
$$

the factor C being introduced for the relaxation of hydrodynamic impedance to particle contact. Hill (1992) argued that the dynamics of thorium in ocean waters and the high contact efficiencies for snowflakes support the idea that C has a high value. Because there are no empirical measurements for this factor, it was decided that for this paper a fixed intermediate value of 100 would be used. As shown below, the diel behaviour of marine snow is not sensitive to this parameter.

The coefficient α which appears in equation (2) is the probability that two aggregates remain stuck together after contact. α is independent of the size of the interacting aggregates for large aggregates (Alldredge and McGillivary, 1991). The empirical values measured for α are variable and depend on the physiological state of the algae forming the aggregates (Kiørboe et al., 1990; Kiørboe and Hansen, 1993). In the current paper this parameter does not depend on the physiological status of phytoplankton cells as the dependence is not yet clear (Kiørboe and Hansen, 1993). Thus, a constant intermediate value of 0.2 was assumed for this parameter (Kiørboe and Hansen, 1993).

Direct implementation of equation (2) in a model of particle dynamics was computationally inefficient because of the large number of size classes involved (see Jackson, 1990; Riebesell and Wolf-Gladrow, 1992). For this reason the first particle models covered only a small range of aggregate sizes. This problem has been overcome in recent models by the use of two different approaches. Hill (1992) defined coefficients that account for the fact that when two particles of a certain nominal size aggregate, they do not generally form a particle whose size corresponds to a nominal size class. Jackson and Lochmann (1992) proposed the use of the mathematical tool developed by Gelbard et al. (1980) to modify the coefficients K_{ij} so that they could be used in size classes on a logarithmic scale. The new coefficients, the sectional kernels, allow the modelling of a wide range of aggregate sizes. In this study the integrals provided by Jackson and Lochmann (1992) were performed, however, rather than integrating K_{ij}, the product $E_{ij}K_{ij}$ was integrated. These kernels include, not only the mechanism by which two particles are brought into proximity, but also the probability that, once the particles are close they collide. Although the calculation of the sectional kernels takes a computational effort, their values are independent of particle concentration and need to be calculated only once for each turbulence level.

Thus, the aggregation coefficients $^1\beta_{kij}$, $^2\beta_{ki}$, $^3\beta_{kk}$ and $^4\beta_{ki}$ appearing in the aggregation term [see equation (23)] result from calculating the integrals described by Jackson and Lochmann (1992) in the expression:

$$
K_{ij(sedim)}E_{ij(sedim)} + K_{ij(shear)}E_{ij(shear)}
\tag{8}
$$

The expression was numerically integrated by using gaussian quadrature (Press et al., 1988). By this procedure, particle sizes between 20 μm and 5 cm were covered with 18 size classes.

Break-up

Break-up terms are not usually included in particle models. One reason for this is the lack of an appropriate set of equations which reflect the kinetics of aggregate break-up. Another reason is the confidence in the capacity of particle models to conserve mass even without a break-up term. However, a break-up term is needed in particle models both for conserving the mass and to improve predictions on particle dynamics through modelling (Ruiz and Izquierdo, in press). The break-up term used in this paper is described in Ruiz and Izquierdo (in press). The rupture of different sized aggregates is considered to be controlled by three different facts. Turbulence exerts stronger shear forces on bigger aggregates, big aggregates are weaker than smaller ones because of their increased porosity, and the rate of rupture of an aggregate depends on the position of the rupture in the aggregate. This is encompassed in the terms r_k, representing the decay rate of particles in size class k due to break-up; and t_{ki}, representing the rate of production of aggregates in size class k due to the rupture of aggregates in class i (Ruiz and Izquierdo, in press). A value of $3.4 \, cm \, s^{-1} \, dyn^{-1}$ was used for the user-defined parameter in the Ruiz and Izquierdo model (H in this paper). This value was higher than that described in Ruiz and Izquierdo (in press) due to the growth term implemented in this model, which increased the size of the aggregates and, therefore, required higher break-up rates in order for the model to conserve mass. The formulae for r_k and t_{ki} are:

$$r_k = \int_{d_{k-1}}^{d_k} \frac{1}{m(\eta)(d_k - d_{k-1})} \left\{ \int_0^{\eta/2} J(\eta, x)[\delta_{b1}(\eta, x)l(\eta, x) + \delta_{b2}(\eta, x)(m(\eta) - l(\eta, x))]dx \right\} d\eta$$

$$t_{ki} = \int_{d_{i-1}}^{d_i} \frac{1}{m(\eta)(d_i - d_{i-1})} \left\{ \int_0^{\eta/2} J(\eta, x)[\delta_{g1}(\eta, x)l(\eta, x) + \delta_{g2}(\eta, x)(m(\eta) - l(\eta, x))]dx \right\} d\eta$$

$$J(\eta, x) = H \frac{\pi\mu(\varepsilon(R)/\nu)^{\frac{1}{2}}(\eta^2/2 - x\eta)}{((\eta/2)^2 - x^2)(1 - P)^{\frac{2}{3}}}$$

$$l(\eta, x) = \left(\frac{\eta - 3x}{2\eta} + \frac{2x^3}{\eta^3} \right) m(\eta)$$

$$(9)$$

where $m(\eta)$ is the nitrogen content of an aggregate of diameter η. The functions δ are the conditional functions described in the Ruiz and Izquierdo (in press) model.

Growth

The growth term included in the model was a light spectrally-averaged model for photosynthesis proposed by Anderson (1993). The model calculated the instantaneous growth rate of phytoplankton averaged over the mixed layer. To do that, it divided the mixed layer into three sub-layers whose depth limits were (0–5 m), (5–23 m) and (23–M, where M is the depth of the mixed layer). For each of these sub-layers Anderson derived spectrally averaged parameters, which were necessary to find the depth-integrated primary production in the mixed layer. This depth-integrated production (Y) is obtained as follows:

$$Y = \sum_{L=1}^{n} \sum_{x=1}^{\infty} \frac{cP_m^B}{k_L} \frac{(-1)^{x+1}}{x \cdot x!} \left[\left(\frac{\alpha_m^B a_L^\# I_{L1}}{P_m^B} \right)^x - \left(\frac{\alpha_m^B a_L^\# I_{L2}}{P_m^B} \right)^x \right] \qquad (10)$$

where n is the number of sub-layers into which the mixed layer is divided (the maximum value equals 3 if $M > 23$), c is concentration of chlorophyll, P_m^B is assimilation number, α_m^B is the maximum photosynthetic efficiency, k_L is the spectrally averaged attenuation coefficient of layer L and $a_L^{\#}$ is a new spectrally averaged photosynthetic parameter derived in the Anderson (1993) model. I_{L1} and I_{L2} are the light entering and leaving layer L respectively, calculated according to the following:

$$I_{L1} = I_0 \exp\left\{\sum_{i=1}^{L-1} -k_i(u_i - u_{i-1})\right\}$$

$$I_{L2} = I_{L1} \exp\left\{-k_L(u_L - u_{L-1})\right\}$$

(11)

for $L > 1$ and u_0, u_1, u_2 and u_3 equal to 0, 5, 23 and M m respectively. I_0 is irradiance at the ocean surface. This was calculated using the usual astronomical formulae (Brock, 1981) to find the light at the top of the atmosphere and by applying the Okta model proposed by Dobson and Smith (1988) for the light transmitted through the atmosphere (a clear sky was assumed). A value of 0.96 was used for transmitance at the air–water interface (Smith and Baker, 1981). Therefore, the photosynthetically active radiation just beneath the ocean surface (I_o) is:

$$I_o = 0.96\,RT$$
$$T = b_1 + b_2 S$$

(12)

where R is photosynthetically active radiation at the top of the atmosphere, T is the atmospheric transmission factor and S is the sine of solar elevation. The constants b_1 and b_2 had a value of 0.4 and 0.386 respectively as in the Okta model of Dobson and Smith (1988) for a clear sky.

The depth-integrated primary production in the mixed layer was divided by the depth-integrated biomass and multiplied by a Michaelis–Menten term for nitrate limitation to obtain the growth rate of phytoplankton (g). The value for the half-saturation constant of the Michaelis–Menten term, P_m^B and α^B (the initial slope of the P–I curve necessary to calculate α_m^B were the same as in Fasham et al. (1990).

Phytoplankton division within an aggregate can increase the size of the aggregate, thus producing a transfer of mass towards larger size classes (Jackson, 1995). To model this phenomenon a function $N(m, t)$ can be used, such that $N(m, t)\,dm$ is the number concentration of particles within the individual mass interval $(m, m + dm)$ at time t. $N(m, t)$ is usually represented through a power function (Rodriguez and Li, 1994):

$$N(m, t) = b_3\,m^{b4}$$

(13)

The particles located at time $t + \delta t$ in mass interval $(m, m + dm)$ are particles that were in the interval $(m^*, m^* + dm^*)$ at time t. If all the phytoplankton growth (except that of individual cells) increases the size, rather than the number, of aggregates it must happen that:

$$N(m, t + \delta t)dm = N(m^*, t)dm^* = N(me^{-g\delta t}, t)e^{-g\delta t}dm$$

(14)

where the equality $m^* = m\,e^{-g\delta t}$ has been used. The time-changing biomass in size class k will then be:

$$Q_k(t + \delta t) = \int_{m_{k-1}}^{m_k} N(m, t + \delta t)m\,dm = \int_{m_{k-1}}^{m_k} N(me^{-g\delta t}, t)e^{-g\delta t}m\,dm$$
$$= \left[e^{-g\delta t(b_4+1)}Q_k(t) \right] \tag{15}$$

Consequently:

$$\frac{dQ_k}{dt} = -g(b_4 + 1)Q_k \tag{16}$$

At each size class $(b_4 + 1)$ was approximated through the following algorithm:

$$(b_4 + 1) = \frac{\log\left(\frac{N_{k+1}}{N_{k-1}}\right)}{\log(m_{k+1}m_k)} \tag{17}$$

except for the smallest size class, in which all the growth goes to increase the number of aggregates, and the largest, in which $(b_4 + 1)$ is assummed to have the same value as in the previous class.

Grazing

The grazing function implemented in this study was that described in Fasham *et al.* (1990) with the difference that it was only non-zero during the night time and only affected aggregates smaller than 0.02 cm. As such, it represented zooplankton up to the size of macrozooplankton (0.2 cm), which were able to graze on particles up to one-tenth of their body size (Longhurst, 1990). The equation implemented is:

$$G_k = \left(\frac{Q_k}{B_{(agg<0.02cm)}} \right)g_r Z \frac{B_{(agg<0.02cm)}}{K + B_{(agg<0.02cm)}} \tag{18}$$

where G_k is the rate of biomass loss in a given size class and $B_{(agg<0.02\ cm)}$ is the mass of aggregates smaller than 0.02 cm. g_r and K are the maximum specific grazing rate and the half-saturation constant for grazing, respectively, with values from Fasham *et al.* (1990). For the size class k, the factor within parentheses shows the dependence of the grazing on concentration relative to $B_{(agg<0.02\ cm)}$. The zooplankton growth equation [see equations (23) and (25)] also included the zooplankton mortality rate (μ_z) and assimilation efficiency (σ_z) which had the same value as in Fasham *et al.* (1990) $(\mu_z = 5.8 \times 10^{-7}\ s^{-1}; \sigma_z = 0.75)$.

This grazing function represented the maximum for zooplankton diel variation in grazing since all the zooplankters migrate to feed during the night. Using this formula we were able to test whether zooplankton had the potential (in the case that the whole zooplankton community migrates daily) to generate diel variations in marine aggregate concentration.

Sedimentation

The sedimentation term used Stokes' law to find the settling velocity of an aggregate as a function of its size. This law produces results that are consistent with empirical records for the whole range of aggregate sizes, provided changes in density resulting from changes in the porosity of aggregates are accounted for (Fig. 1). Thus, Stokes' law could be formulated for the case of marine aggregates as (Tambo and Watanabe, 1979):
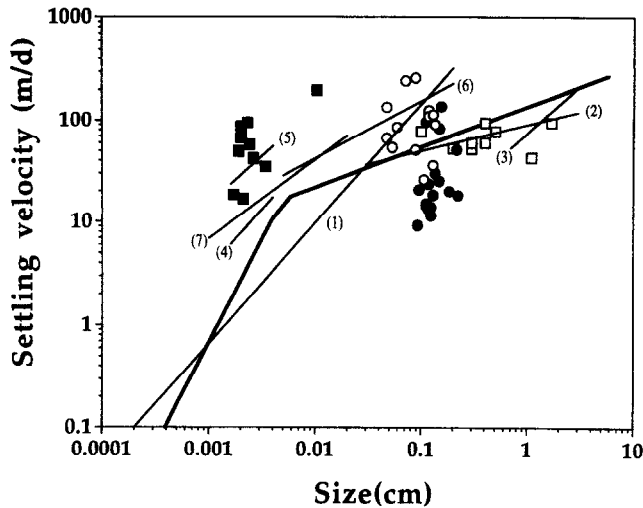
Fig. 1. Size dependence of aggregate sinking velocities. Empirical results compared with Stokes' law. The symbols represent: empty circles, Azetsu-Scott and Johnson (1992) Bedford Basin aggregates; filled circles, Azetsu-Scott and Johnson (1992) aggregates from diatom cultures; empty squares, Shanks and Trent (1980); filled squares, Carder et al. (1982). The different numbers marking the lines are: 1, Jackson (1989); 2, Alldredge and Gotschalk (1988); 3, Alldredge and Gotschalk (1989); 4, Hawley (1982) population A; 5, Hawley (1982) population B; 6, Kajihara (1971); 7, Gibbs (1985). The thick line is Stokes' terminal velocity.

$$w = \frac{2}{18\mu}(1 - P)(\rho_c - \rho_w)ad^2 \qquad (19)$$

where d is the aggregate diameter, w is the sinking velocity, μ is the dynamic viscosity, P is the porosity of the aggregate, a is the gravitational acceleration, ρ_c is the density of constituent matter and ρ_w is sea water density (1.0217 g cm^{-3} in this model).

The density of the constituent matter (ρ_c) depends on the material from which the aggregate is made. Azetsu-Scott and Johnson (1992) measured the constituent matter density of aggregates from diatom cultures and from Bedford Basin by using a density gradient column, and found values ranging from 1.095 to 1.497 g cm^{-3}. Alldredge and Gotschalk, 1988 assumed 1.2 g cm^{-3} to be the value of constituent density of marine aggregates, a value within the range measured by Azetsu-Scott and Johnson (1992). However, a slightly lower value (1.17 g cm^{-3}) produced better agreement between Stokes' law and the empirical observations (see below).

The relationship between the porosity and size of an aggregate is (Alldredge and Gotschalk, 1988):

$$(1 - P) = 8 \times 10^{-3}d^{-1.6} \qquad (20)$$

where d is the diameter in mm. This equation was calculated from aggregates with sizes ranging from 300 µm to 2 cm. An extrapolation of this equation to sizes smaller than 50 µm would result in negative values of porosity, which are not possible. Since in the present study there was no information on the porosity of aggregates smaller than 300 µm, it was assumed that equation (20) was valid for aggregates down to 50 µm in size. For aggregates smaller than 50 µm it was assumed that the porosity was zero.

The discrepancy between Stokes terminal velocity and some of the results displayed in Fig. 1 was due to the difference between the constituent matter density accepted for this model and that of the aggregates. Carder *et al.* (1982) and Azetsu-Scott and Johnson (1992) (aggregates from Bedford Basin) reported the presence of mineral particles within their aggregates. Mineral particles were also expected in the aggregates of Hawley (1982) as well as in those studied by Kajihara (1971) and Gibbs (1985), since they were collected near sediments or in bay waters. Mineral particles have a density much higher than the constituent density assumed in this paper and, consequently, produce faster settling velocities for the aggregates. There was also a discrepancy between the results of the current model and the empirical results from the diatom aggregates of Azetsu-Scott and Johnson (1992). This discrepancy cannot be explained at present, however the results reported by Azetsu-Scott and Johnson (1992) are very low when compared with the rest of the aggregates displayed in Fig. 1.

Once the settling velocity of aggregates is known, the loss term representing the settling of aggregates is:

$$-\frac{w_k}{M}Q_k \tag{21}$$

where w_k and Q_k are the sinking velocity and mass concentration of class k respectively. M is the depth of the mixed layer (40 m in this model).

Nitrogen content of aggregates

The size dependence of the aggregate porosity had a strong effect, not only on aggregate sinking rates, but also on the amount of organic matter transported by each aggregate when sinking into the deep ocean. The amount of carbon or nitrogen in each aggregate (m_k) is:

$$m_k = \theta\rho_c(1 - P)V_k \tag{22}$$

where $(1 - P)$ is size-dependent [equation (20)], and θ is the carbon or nitrogen proportion of the constituent matter. The value of θ used for nitrogen in this model is 0.01, corresponding to organic matter having a dry weight that is 10% of the wet weight, and 10% of dry weight being composed of nitrogen. V_k is the nominal volume of particles in size class k. Appropiate conversion factors were used in equation (22) to transform from grams of N to µmoles of N. The nitrogen content estimated using equation (22) agreed with that recorded for aggregates of the same size (Shanks and Trent, 1980). Thus, size-dependent porosity was a good tool for describing, not only the sinking speed of aggregates, but also their nitrogen or carbon content. As in the case of sinking velocity, there was no information on the composition of small marine aggregates.

Transparent exopolymer particles

The presence of transparent exopolymer particles (TEP) was not modelled in this paper. The importance of these particles has become apparent in several papers (Alldredge *et al.*, 1993; Passow *et al.*, 1994). They act as a matrix for the sticking of phytoplankton cells, thereby favouring the aggregation of these cells. As more information becomes available on their characteristics and rates of production, their modelling and inclusion in future particle models will allow predictions of aggregate concentrations which are closer to those observed

in the field. In any case, TEP did not display any apparent daily cyclic behaviour in the studies performed so far, as their dynamics seem to be associated with the growth and aging of phytoplankton populations, which have a time scale of several days (Alldredge *et al.*, 1993; Passow *et al.*, 1994). Therefore, the inclusion of TEP in the model would not alter the cyclic pattern of particulate matter described in this paper.

Governing equation

The total equation is:

$$
\begin{aligned}
\frac{dQ_k}{dt} = {} & \frac{\alpha}{2}\sum_{i=1}^{k-1}\sum_{j=1}^{k-1}\overline{^1\beta_{kij}}Q_iQ_j - \alpha Q_k\sum_{i=1}^{k-1}\overline{^2\beta_{ki}}Q_i \\
& -\frac{\alpha}{2}\overline{^3\beta_{kk}}Q_k^2 - \alpha Q_k\sum_{i=k+1}^{18}\overline{^4\beta_{ki}}Q_i \qquad\qquad AGGREGATION \\
& -r_kQ_k + \sum_{i=k+1}^{18}t_{ki}Q_i \qquad\qquad\qquad BREAK-UP \\
& -g\frac{\log\left(\frac{N_{k+1}}{N_{k-1}}\right)}{\log(m_{k+1}m_k)}Q_k \qquad\qquad GROWTH \\
& -f(R)G_k \qquad\qquad\qquad\qquad\quad GRAZING \\
& -\frac{w_k}{M}Q_k \qquad\qquad\qquad\qquad\quad SEDIMENTATION
\end{aligned}
$$

(23)

where $f(R)$ is zero for $R > 0$ and 1 for $R = 0$.

The equation for nitrogen (N_o) is:

$$
\frac{dNo}{dt} = -\sum_{k=1}^{18}gQ_k
$$

(24)

And the equation for zooplankton is:

$$
\frac{dZ}{dt} = \sum_{k(d_k<0.02\text{cm})}\sigma_z f(t)G_k - \mu_z Z
$$

(25)

The different size classes were obtained by arranging the particle sizes in a geometrical scale in which the upper bound of each size class is twice the mass of the lower bound. For the lower bound of the smallest size class, the nominal mass of a solitary alga of 20 μm equivalent spherical diameter was used. The system of differential equations was numerically integrated by using the Runge–Kutta–Fehlberg adaptative time step method with a local truncation error below 10^{-3} μM of N (Kincaid and Cheney, 1991).

RESULTS

Four different versions of the model described above (models 1 to 4) were run to investigate which mechanism was responsible for the daily cycles of marine aggregates. Model 1 had neither grazing nor turbulence cycles. In this way it was possible to test whether

the daily cycles of phytoplankton production were responsible for cyclic behaviour of marine aggregates. Model 2 was the same as model 1 but with a daily cycle of grazing (turbulence is not cyclic). The same growth function as in model 1 was used since, as explained below, growth did not generate cycles in aggregates. This model tested whether zooplankton were the cause of daily cycles of marine aggregates. Model 3 was the same as model 1 but with cycles of turbulence. In this way, it was possible to test whether turbulence was the cause of the cyclic behaviour of marine aggregates. Finally, model 4 incorporated the three cycling processes (growth, grazing and turbulence) to check for any possible synergistic effect in the generation of diel cycles of aggregate concentration.

The four models were run for a three-month simulation that began in May. The initial nitrate concentration (8 μM) generated a phytoplankton bloom in the four models (Fig. 2). In models 2 and 4, the phytoplankton concentration became very low at the end of June because of grazing pressure. Aggregate concentration in the four models had a peak that coincided with the phytoplankton peak. This peak was highest in model 1 and lowest in
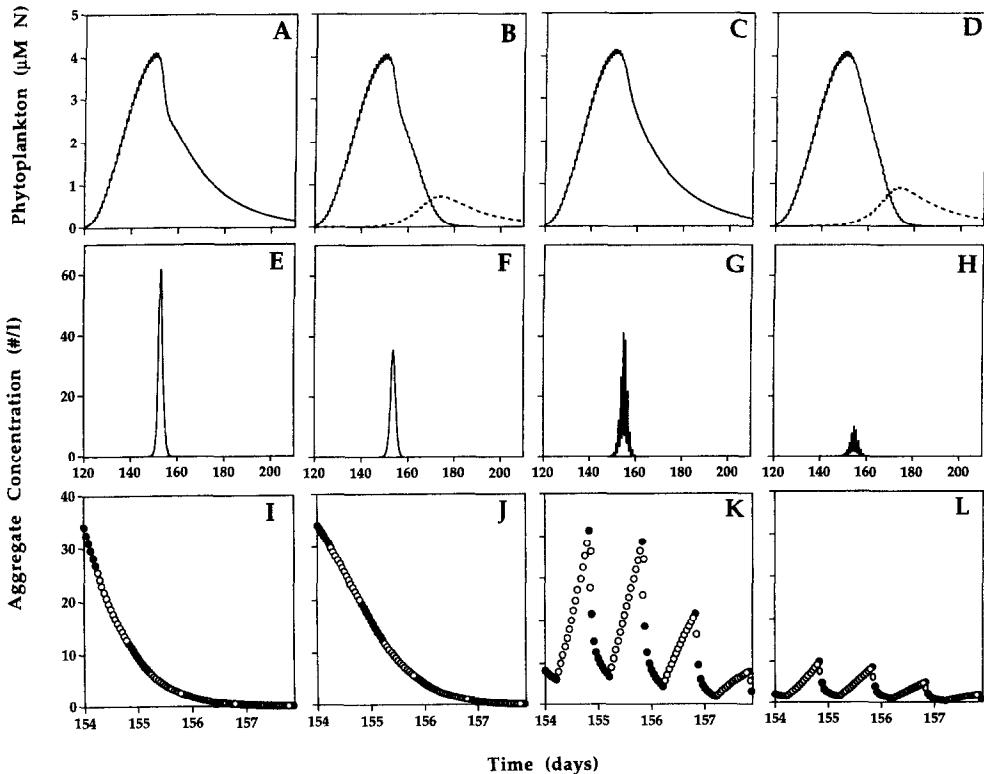

Fig. 2.   Time evolution of phytoplankton and aggregate concentration for the four different models. The four columns represent models 1, 2, 3 and 4 respectively (see text). The three rows represent phytoplankton concentration, aggregate number concentration (larger than 500 μm) and an expanded view of the evolution of the aggregate number concentration, respectively . For instance, figure F represents the evolution of aggregate number concentration along the time series for model 2. The dashed line of figures B and D is the evolution of zooplankton concentration. In the third row (figures I, J, K and L), empty circles are for day-time and filled circles are for night-time.

model 4. Models 3 and 4 also displayed greater vertical variability than models 1 and 2 in the evolution of aggregate concentration. The detailed evolution of aggregate concentration on a scale of days (third row) revealed the origin of the higher vertical variability in models 3 and 4. It was evident that daily cycles in the concentration of marine aggregates occured only in those models which had daily cycles of turbulence. The daily cycles of fluxes from the mixed layer also only appeared in models 3 and 4. As an example of the evolution of these cycles, Fig. 3 shows them for models 2 and 4. It is evident from the graph that only the model with oscillating turbulence (model 4) had vertical scatter resulting from diel variability.

Power spectra analysis of the results obtained from the four models highlighted cyclical behaviour. A summary of the power spectra analysis of the different models is presented in Table 1. It shows the percentage of variance in the total time series that is contained in frequencies between 0.9 and 1.1 d^{-1}. The only models in which a substantial percentage of variance was contained within this band were those for which turbulence has a diel change, i.e. models 3 and 4.

Different initial conditions and modification of the submodels were used to check for the
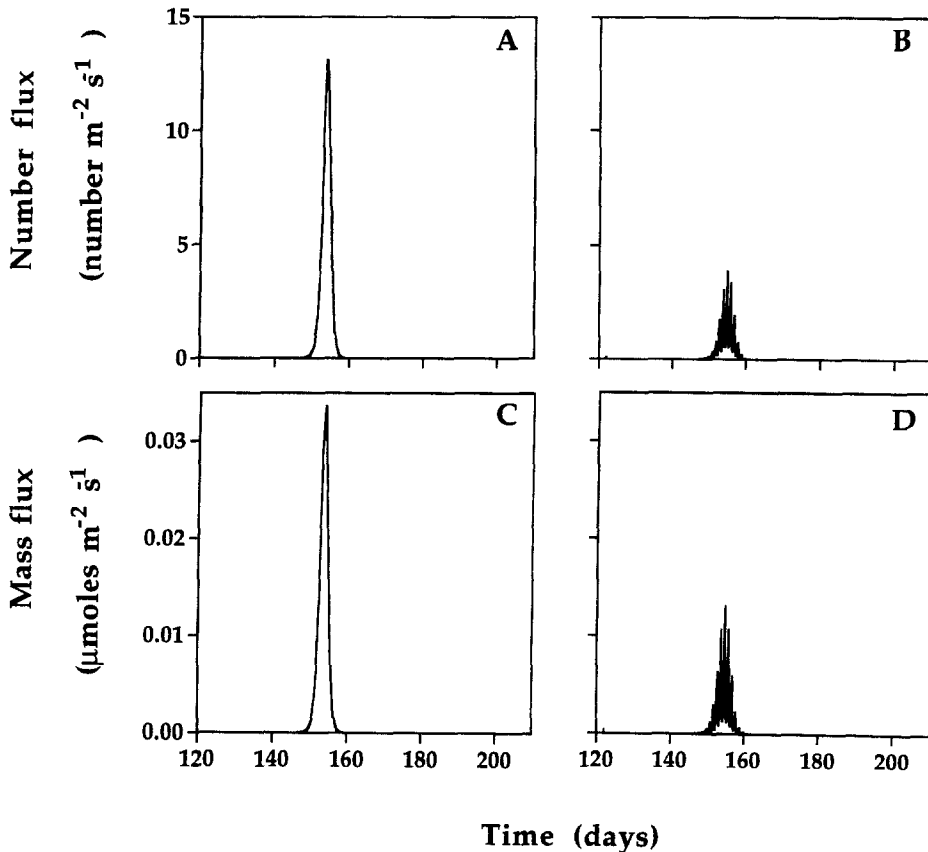

Fig. 3. Time evolution of aggregate number and mass flux from the mixed layer. First and second column are respectively the results of models 2 and 4. First and second row are respectively number and mass flux.

Table 1.   *Percentage of variance between frequencies 0.9 and 1.1 day^{-1} for the different models and variables analysed*

	Model 1	Model 2	Model 3	Model 4
Phytoplankton biomass	0.01	0.01	0.01	0.01
Aggregate number concentration	0.01	0.01	15.33	16.35
Aggregate mass concentration	0.01	0.01	17.80	18.78
Aggregate number sedimentation	0.01	0.01	16.54	17.54
Aggregate mass sedimentation	0.01	0.02	20.71	21.68

sensitivity of the results to some of the model assumptions. Thus, in the results presented above, model 2 was run with an initial zooplankton biomass which allowed development of the phytoplankton bloom. If this initial zooplankton concentration was set high enough, it resulted in the prevention of high concentrations of algal aggregates during the simulation, but in negligible aggregate cycles. The sensitivity of aggregate cycles to the levels of oscillating turbulence was tested by running model 3 with a smaller diel change in turbulence levels, ε changing between 5×10^{-9} and 5×10^{-8} m^2 s^{-3} for the day and night respectively. This involved a variation of one order of magnitude, about the minimum range described by Brainerd and Gregg (1993), and resulted in a percentage of variance between 0.9 and 1.1 d^{-1} of 7.19 for number and 8.36 for mass concentration of aggregates.

Sensitivity to the break-up term used was also tested by using a much simpler term which was similar to that implemented by Hill (1992), i. e. particles reaching the largest size class stay in that class and do not form bigger ones. With this break-up term the percentage of variance embraced between 0.9 and 1 d^{-1} was 0.85 for number concentration and 28.91 for mass concentration. The low variance in number and high variance in mass concentration was the consequence of the accumulation by this model of aggregates in the largest size class in which numbers of particles were small but the masses were high. Another break-up term was also tested by implementing the model described in Jackson (1995), the break-up of each size class equals $b_5 b_6{}^k$ (where b_5 and b_6 are empirically fitted parameters and k is the number of the size class). This formula was used for size classes in which the upper boundary of each class was twice the mass of the lower boundary and assumed that the mass of size class k went to size class k − 1. The parameter b_6 is dimensionless (which was necessary for dimensional consistency of the rate of different size classes) and implies that the ratio between the break-up rate of consecutive size classes equals 1.45. This term was implemented in model 3 using the same value for b_6 but fitting the value of b_5 (which depends on the correspondence between the numeration given to a certain class and the particle sizes included in that class) as in the model to produce a sensible aggregate concentration during the bloom ($b_5 = 2.044$ d^{-1}). This produced a percentage of variance between 0.9 and 1.1 d^{-1} of 17.70 for number and 15.57 for mass concentration. The implementation of this break-up term in model 2 ($b_5 = 2.399$ d^{-1}) produced a percentage of variance of 0.18 for number and 0.21 for mass concentration, thereby confirming the turbulent origin of the cycles when using an empirical break-up term. Besides different break-up terms, the sensitivity of the cycles to different values of H, the user-defined parameter in the Ruiz and Izquierdo (in press) model was also tested. Thus, model 3 was run with a high (3.5 cm s^{-1} dyn^{-1}) and a low (3.3 cm s^{-1} dyn^{-1}) value for this parameter. The aggregate concentration predicted by the model was very sensitive to these variations in H

and the maximum values achieved during the bloom were 7 and 114 aggregates l^{-1} for high and low values of H respectively (about three times lower and higher than the concentrations produced by the standard model 3 in which $H = 3.4$ cm s^{-1} dyn^{-1}). Despite the high variation in concentrations, the cyclic behaviour of marine aggregates was not sensitive to H. In the case of high values of H, the percentage variance between 0.9 and 1 d^{-1} was 17.06 for number and 19.48 for mass concentration. For low H values, this percentage was 12.97 for number and 15.45 for mass concentration.

The sensitivity of the results to the aggregation term implemented was also tested. Thus, of the two terms included in the aggregation submodel, shear dominated over differential sedimentation. This could result in an overestimation of the role of turbulence oscillations in the dynamics of aggregates and therefore in the generation of diel cycles. This possibility was explored by running model 3 with a different version of the aggregation kernels, in which no efficiencies [equations (5) and (6)] were included. In such a way aggregation by differential sedimentation was higher than aggregation by shear and it could be checked whether the observed diel changes were the result of using a set of kernels in which shear predominated over differential sedimentation. This resulted in percentage variances of between 0.9 and 1 d^{-1} of 10.52 for number and 10.74 for mass concentration of aggregates, therefore demonstrating the persistence of this pattern. The response of the model to different values of the constant C was also tested. Model 3 produced percentage variances of 15.89 for number and 17.95 for mass concentration when $C = 50$. When $C = 200$ these percentages were 13.79 for number and 16.44 for mass concentration.

The size distribution of particles produced by the complete model (model 4) is shown in a normalized fashion in Fig. 4 (Platt and Denman, 1977) for days 155 and 170 of the time series. The spectra are close to linear when represented on a log–log scale and become less
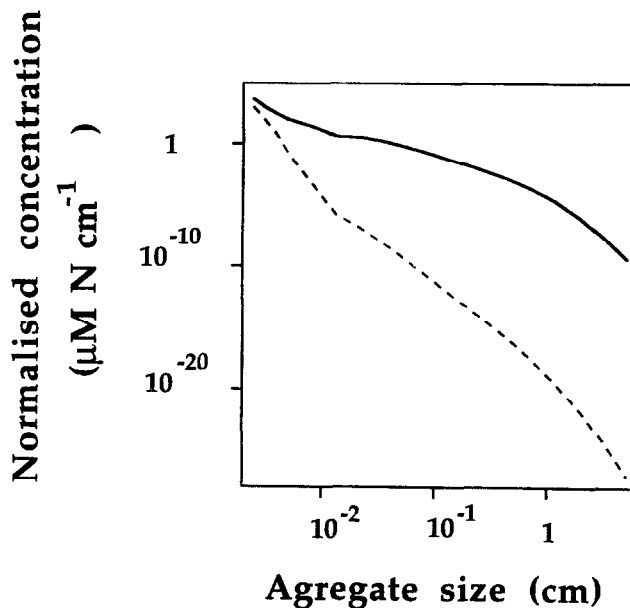

Fig. 4. Normalized spectra for the mass concentration of aggregates. Solid and broken lines represent the spectra resulting from days 155 and 170 of the time series respectively.

steep during the bloom period. This is also noticeable in Fig. 5, which shows the evolution of the slope of the log–log linear model for the time period in which the number of aggregates presented in the different size classes allowed its calculation. Figure 5 shows the existence of daily cycles in the slope, demonstrating again the important diel influence of variations in turbulence, not only on the total particle concentration, but also on the size structure of the pelagic particle population. The slopes predicted by the model were lower than those usually found for pelagic particles (Sheldon et al., 1972; Platt and Denman, 1977; Rodriguez and Li, 1994), possibly because the model underestimated the proportion of large particles in seston or because of the differences in the size range studied.

The smearing of the diel pattern of surface marine snow in travelling from the base of the mixed layer to 270 m depth was explored using a simple finite difference scheme coupled to model 4. In this simplified scheme, the particles leaving the mixed layer did not aggregate and each class was allowed to settle at the velocity described in equation (19). The results for the number and mass concentration of marine snow are presented in Fig. 6, and show a diel behaviour at this depth. The time lag between the aggregate peak at the surface and at 270 m depth was about 6 days. The percentage of variance between 0.9 and 1.1 d^{-1} was smaller than at the surface (0.57 for number and 1.16 for mass concentration), but the shape of the power spectra (not shown) displayed a clear peak at frequencies of 1 d^{-1}, as shown in Lampitt et al. (1993a). Figure 6 also shows the dynamics of aggegates separated into those that are bigger or smaller than 1 mm. Both types of aggregate displayed daily cycles that were more apparent for large aggregates which had a shorter time lag after the peak in the surface, around 2–3 days.

DISCUSSION

The existence of a diel pattern of marine snow was unknown before Lampitt et al. (1993a). This work posed the question, what is the mechanism that generates the cycles?
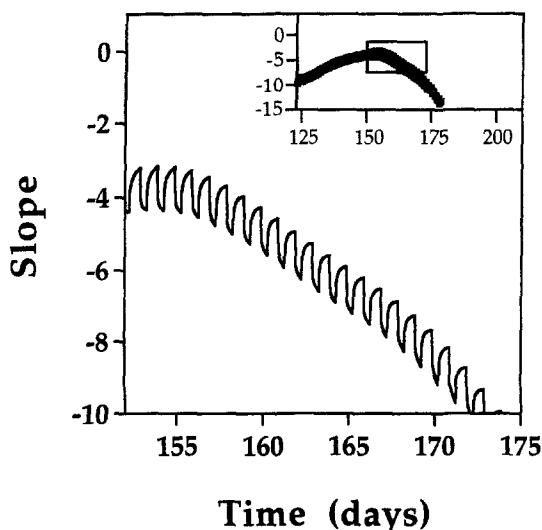

Fig. 5. Evolution of the slope that can be fitted to the normalized mass spectra when represented in a log–log scale. The small figure in the upper right side is the evolution along the whole time series.
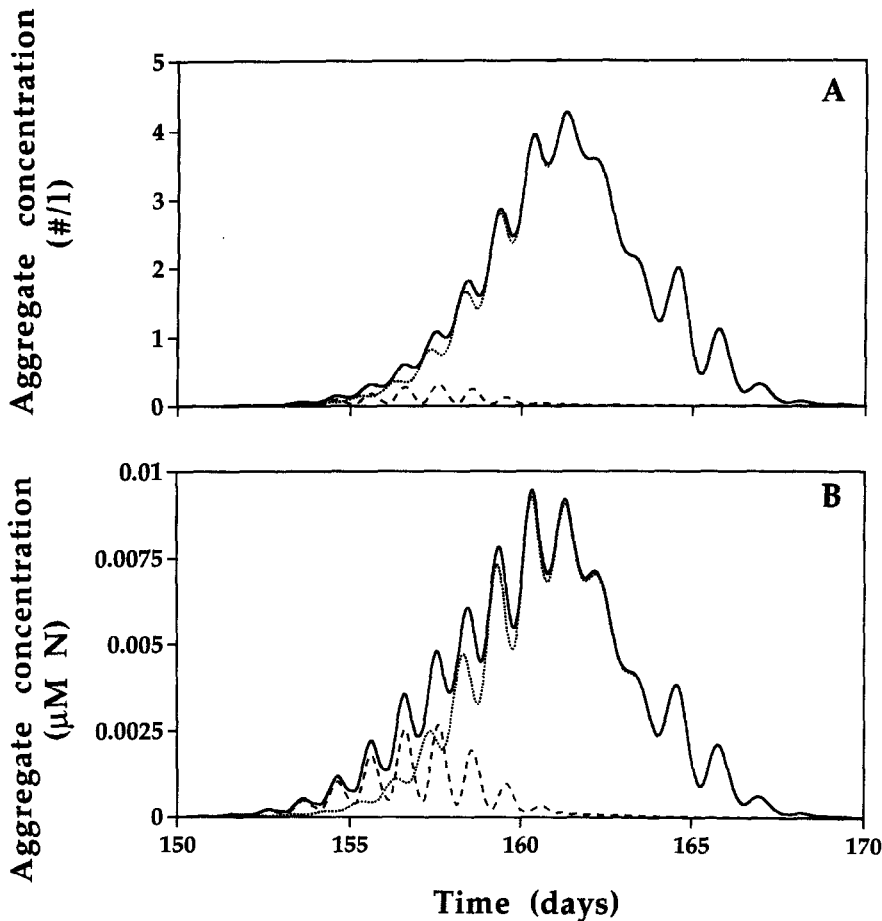
Fig. 6.   Aggregate number (A) and mass (B) concentration at 270 m depth along the time series. The
solid line shows the concentrations of aggregates larger than 500 μm for the period of the total series
in which the concentrations were high. The dotted line represents aggregates between 500 μm and
1 mm. The broken line represents aggregates larger than 1 mm.

Zooplankton is one possible cause since many zooplankters have daily vertical migrations in which they rise to shallower waters during the night and sink to depth during the day (Longhurst, 1976). This behaviour might create a daily cycle of marine aggregates as a result of the grazing pressure exerted by zooplankters during the night. There are two other mechanisms that are important in the dynamics of particulate matter in sea water and which present daily cycles. These are the cycles of growth and turbulence in the mixed layer that result from the daily cycles of solar radiation. On the one hand, daily cycles of growth impose a daily cycle of matter input to the pelagic ecosystem. On the other hand, daily cycles of turbulence are also a good candidate for the production of daily cycles in marine aggregates. The presence of such cycles of turbulence in the mixed layer is a phenomenon that has become apparent following reliable measurements of turbulent kinetic energy in the upper ocean (Brainerd and Gregg, 1993). These cycles result from the daily cycle of radiation on the ocean surface. Thus, during the day the surface of the ocean is heated,

consequently it becomes stratified, and this stratification decreases turbulence levels. During the night the surface of the ocean cools, provoking a convective release of potential energy as turbulent kinetic energy. Consequently, turbulence levels rise during the night. In fact, the process is more complex than explained above and the water column, above the seasonal thermocline, has spatial heterogeneity. Usually, two layers can be observed: a well-mixed layer at the ocean surface and a remnant layer below it (Brainerd and Gregg, 1993). The turbulence values reported by Brainerd and Gregg (1993) for the remnant layer are considered in this paper. The remnant layer occupies a great portion of the water column above the seasonal thermocline and the turbulence levels measured are not contaminated by a ship's wake.

The model described in this paper can be used to test which of the three processes described above is able to generate marine aggregate cycles. The model incorporates a light-dependent instantaneous growth rate, a grazing function that can be switched on and off every day and finally, not only an aggregation term for marine particles, but also a break-up term. By including this term, the final effect that turbulence has in the dynamics of particulate matter is not only an increase in the aggregation rate (due to increasing shear levels), but also the result of both aggregation and break-up. Other characteristics of the model are that it is able to cover a wide range of aggregate sizes and that both the settling velocities and nitrogen content of the particles are consistent with existing measured values.

From the four different versions of the model (see the results section), three main conclusions can be reached:

First, daily cycles of phytoplankton growth produce negligible daily cycles of marine aggregates. Despite the importance of these growth cycles in the dynamics of phytoplankton, the oscillations they generate in the concentration or flux of marine snow are small.

Second, daily cycles of zooplankton grazing produce negligible daily cycles of marine aggregates. Including a grazing function that is switched on only during the night increases the daily cyclic behaviour of phytoplankton. This results from phytoplankton concentration increasing only during the day while during the night its concentration decreases not only by sedimentation, as in model 1, but also because of grazing. However, even in this case, the daily cyclic behaviour of phytoplankton concentration does not produce associated daily cycles of algal aggregates. The grazing function implemented in the model is a maximum case in the sense that the whole zooplankton community has a daily grazing cycle. However, this is not the case (Valiela, 1984). Therefore, even in the maximum case, zooplankton grazing cannot generate cycles of algal aggregates.

Third, daily cycles of mixed-layer turbulence do produce daily cycles of aggregates in the mixed layer. Thus, cycles in turbulence levels produce cycles in both the number and mass concentration of aggregates in the mixed layer as well as a daily cycle of aggregates leaving the mixed layer. The diel variations in aggregation dynamics generated by turbulence makes this process a good candidate for explaining the diel variations reported by Lampitt *et al.* (1993a).

Although these conclusions are based on the simplified version of reality of a model, the capacity of turbulence to generate diel changes in aggregate concentration has proved to be robust to different submodels for aggregation and break-up. This robust pattern is a consequence of the high diel variation of turbulence levels in the mixed layer (Brainerd and Gregg, 1993) and of the dependence of aggregation and disaggregation rates on these levels. Thus, a variation of ε from 10^{-9} to 7×10^{-8} m^2 s^{-3} implies a rate of aggregation by shear

that is 8.3 times higher during night than during the day for particles smaller than 0.01 cm [the rate depends on $\varepsilon^{1/2}$; equation (4)]. For particles larger than 0.01 cm this factor is 4.1 [the rate depends on $\varepsilon^{1/3}$; equation (4)]. As the break-up rate depends on $\varepsilon^{1/2}$ [equation (9)], this diel change in turbulence also generates break-up rates that are different by a factor of 8.3 between day and night. The diel decrease of marine snow concentration during the night is a consequence of the form that aggregation and break-up of big particles scale with ε, $\varepsilon^{1/2}$ for break-up and $\varepsilon^{1/3}$ for aggregation, which produces higher increases in break-up (compared to aggregation) rates when turbulence rises. The diel changes in aggregate concentration resulting from the dependence of these rates on ε are much higher than those that result from variations of phytoplankton concentration due to growth or grazing. Thus, the maximum diel change in biomass concentration observed in models 1 and 2 never exceeds 10% during the phytoplankton bloom period, in which most of the aggregate variance is generated. This implies that the ratios of aggregation rates driven by changes in phytoplankton concentration vary by $(1.1)^2 = 1.2$, which explains why models 1 and 2 are not able to generate daily cycles of marine snow. The general increase of aggregate size, which results from the diel growth of phytoplankton within aggregates, is also not enough to produce the apparent diel cycles of marine snow.

However, turbulence is able to produce daily cycles even when a range of variation about the minimum described by Brainerd and Gregg (1993) is implemented. Moreover, the cycles of aggregate flux predicted by models 3 and 4 only represent a lower limit for the possible cyclic behaviour generated by turbulence. Thus, as well as the cycles generated by increased aggregation and break-up during the night, turbulence can also generate daily cycles in the sedimentation loss of aggregates which result from variations in their vertical distribution (Ruiz, 1996). These daily changes in vertical distribution, and their corresponding changes in sedimentation rate, are higher for large aggregates (Ruiz, 1996). In addition, the uncertainty that exists in some of the parameters of aggregation and disaggregation models does not affect the fact that both rates increase rapidly with aggregate size, which makes them particularly sensitive to turbulence levels. Therefore, the diel flux of large aggregates must be especially sensitive to turbulence levels since two of the processes controlling it, spatial distribution and aggregation–disaggregation rates, have significant variation depending on these levels. The daily signal in aggregate flux generated at the surface by these processes is not smeared with depth and the diel pattern is still apparent at 270 m, particularly in the case of large aggregates (Fig. 6). Although the smearing of small aggregates while sinking makes their diel pattern less apparent at 270 m than in the surface it still can be observed (Fig. 6). The fact that the diel signal at the surface is not completely destroyed with depth is associated with the effect that porosity has on the sinking of aggregates. Thus, due to the effect of porosity, the settling velocity of porous aggregates depends on $d^{0.4}$ rather than on the much stronger size-dependence of d^2 as expected from Stokes law for non-porous particles. This weak size-dependence prevents a higher smearing the diel signal during sinking.

The importance of turbulence in aggregate cycles, does not imply that variability in phytoplankton growth rates or in zooplankton grazing pressure are not important for controlling the dynamics of marine snow. However, the variability in these processes is more likely to affect marine aggregates on a seasonal time scale. Thus, the control that seasonal cycles of primary production have on the concentration of algal aggregates is clear from both empirical and modelling results. The highest concentrations of these aggregates, in the open ocean, are recorded during phytoplankton blooms that have a seasonal cycle. The

influence of zooplankton on the dynamics of marine snow is also more likely to be related to the seasonal, rather than the daily, cycle of algal aggregates. Zooplankton are a key factor in explaining the seasonal evolution of pelagic ecosystems and the presence, or not, of phytoplankton blooms in ecosystem models (Fasham, 1995). Therefore, zooplankton also exert control on the seasonal evolution of algal aggregates. In this paper it was tested whether a high grazing pressure could inhibit the formation of high concentrations of algal aggregates in the model. However, even in such cases, zooplankton were not able to generate significant daily cycles of aggregates, so it is unlikely that this constitutes the origin of these cycles at the ocean surface.

Consequently, neither daily cycles of growth nor of grazing can explain the daily cycles of algal aggregates observed in the pelagic ecosystem. Turbulence which presents a high daily variability as well as the proven sensitivity of the particle dynamics to changing turbulence is the best candidate to explain these cycles.

REFERENCES

Alldredge, A. L. (1992) Marine snow in oceanic cycling. In *Encyclopedia of Earth System Science*, ed. W. A. Nierenberg, Vol. 3, pp. 139–147. Academic Press, New York.
Alldredge, A. L. and Gotschalk, C. C. (1988) *In situ* settling behaviour of marine snow. *Limnology and Oceanography*, 33, 339–351.
Alldredge, A. L. and Gotschalk, C. C. (1989) Direct observations of the mass flocculation of diatom blooms: characteristics, settling velocities and formation of diatom aggregates. *Deep-Sea Research*, 36, 159–171.
Alldredge, A. L. and McGillivary, P. (1991) The attachment probabilities of marine snow and their implications for particle coagulation in the ocean. *Deep-Sea Research*, 38, 431–443.
Alldredge, A. L. and Silver, M. W. (1988) Characteristics, dynamics and significance of marine snow. *Progress in Oceanography*, 20, 41–82.
Alldredge, A. L., Passow, U. and Logan, B. E. (1993) The abundance and significance of a class of large, transparent organic particles in the ocean. *Deep-Sea Research I*, 40, 1131–1140.
Anderson, T. R. (1993) A spectrally averaged model of light penetration and photosynthesis. *Limnology and Oceanography*, 38, 1043–1419.
Asper, V. L. (1987) Measuring the flux and sinking speed of marine snow aggregates. *Deep-Sea Research*, 34, 1–17.
Azetsu-Scott, K. and Johnson, B. D. (1992) Measuring physical characteristics of particles: a new method of simultaneous measurement for size, settling velocity and density of constituent matter. *Deep-Sea Research*, 39, 1057–1066.
Brainerd, K. E. and Gregg, M. C. (1993) Diurnal restratification and turbulence in the oceanic surface mixed layer. 1 Obsevations. *Journal of Geophysical Research*, 98, 22645–22656.
Brock, T. D. (1981) Calculating solar radiation for ecological studies. *Ecological Modelling*, 14, 1–19.
Carder, K. L., Steward, R. G. and Betzer, P. R. (1982) *In situ* holographic measurements of the sizes and settling rates of oceanic paticulates. *Journal of Geophysical Research*, 87, 5681–5685.
Dobson, F. W. and Smith, S. D. (1988) Bulk models of solar radiation at sea. *Quarterly Journal of the Royal Meteorological Society*, 114, 165–182.
Fasham, M. J. R., Ducklow, H. W. and McKelvie, S. M. (1990) A nitrogen-based model of plankton dynamics in the oceanic mixed layer. *Journal of Marine Research*, 48, 591–639.
Fasham, M. J. R. (1995) Variations in the seasonal cycle of biological production in subartic oceans: a model sensitivity analysis. *Deep-Sea Research I*, 42, 1111–1149.

Fowler, S. W. and Knauer, G. A. (1986) Role of large particles in the transport of elements and organic compounds through the oceanic water column. *Progress in Oceanography*, **16**, 147–194.

Gelbard, F., Tambour, Y. and Seinfeld, J. H. (1980) Sectional representations for simulating aerosol dynamics. *Journal of Colloid and Interface Science*, **76**, 541–556.

Gibbs, R. J. (1985) Estuarine flocs: their size, settling velocity and density. *Journal of Geophysical Research*, **90**, 3249–3251.

Hawley, N. (1982) Settling velocity distribution of natural aggregates. *Journal of Geophysical Research*, **87**, 9489–9498.

Hill, P. S. (1992) Reconciling aggregation theory with observed vertical fluxes following phytoplankton blooms. *Journal of Geophysical Research*, **97**, 2295–2308.

Hill, P. S., Nowell, A. R. M. and Jumars, P. A. (1992) Encounter rate by turbulent shear of particles similar in diameter to the Kolmogorov scale. *Journal of Marine Research*, **50**, 643–668.

Jackson, G. A. (1989) Simulation of bacterial attraction and adhesion to falling particles in an aquatic environment. *Limnology and Oceanography*, **34**, 514–530.

Jackson, G. A. (1990) A model of the formation of marine algal flocs by physical coagulation processes. *Deep-Sea Research*, **37**, 1197–1211.

Jackson, G. A. (1995) Comparing observed changes in particle size spectra with those predicted using coagulation theory. *Deep-Sea Research II*, **42**, 159–184.

Jackson, G. A. and Lochmann, S. E. (1992) Effects of coagulation on nutrient and light limitation of an algal spring bloom. *Limnology and Oceanography*, **37**, 77–89.

Kajihara, M. (1971) Settling velocity and porosity of large suspended particles. *Journal of the Oceanographic Society of Japan*, **27**, 158–162.

Kincaid, D. R. and Cheney, E. W. (1991) *Numerical Analysis*, pp. 690. Brooks/Cole, Belmont.

Kiørboe, T. and Hansen, J. L. S. (1993) Phytoplankton aggregate formation: observations of patterns and mechanisms of cell sticking and the significance of exopolymeric material. *Journal of Plankton Research*, **15**, 993–1018.

Kiørboe, T., Andersen, K. P. and Dam, H. G. (1990) Coagulation efficiency and aggregate formation in marine phytoplankton. *Marine Biology*, **107**, 235–245.

Kranck, K. and Milligan, T. (1988) Macroflocs from diatoms: *in situ* photography of particles in Bedford Basin Nova Scotia.. *Marine Ecology Progress Series*, **44**, 183–189.

Lampitt, R. S., Hillier, W. R. and Challenor, P. G. (1993a) Seasonal and diel variation in the open ocean concentration of marine snow aggregates. *Nature*, **362**, 737–739.

Lampitt, R. S., Wishner, K. F., Turley, C. M. and Angel, M. V. (1993b) Marine snow studies in the northeast Atlantic: distribution, composition and role as a food source for migrating plankton. *Marine Biology*, **116**, 689–702.

Landau, L. D. and Lifshitz, E. M. (1959) *Fluid Mechanics*, pp. 536. Pergamon, London.

Longhurst, A. R. (1976) Vertical migration. In *The Ecology of the Seas*, ed. D. H. Cushing and J. J. Walsh. Blackwell, Cambridge.

Longhurst, A. R. (1990) Pelagic ecology: Definition of pathways for material and energy flux. In *Océanologie, actualité et prospectives. Proceedings of the Centennial of the Station Marine d'Endoume*, M. Denis (ed.). Marseille, pp. 263–288.

Mccave, I. N. (1984) Size spectra and aggregation of suspended particles in the deep ocean. *Deep-Sea Research*, **31**, 329–352.

Passow, U., Alldredge, A. L. and Logan, B. E. (1994) The role of particulate carbohydrate exudates in the flocculation of diatom blooms. *Deep-Sea Research I*, **41**, 335–357.

Platt, T. and Denman, K. (1977) Organization in the pelagic ecosystem. *HelgolSnder wissenshaftliche Meeresuntersuchungen*, **30**, 575–581.

Prézelin, B. B. and Alldredge, A. L. (1983) Primary production of marine snow during and after an upwelling event. *Limnology and Oceanography*, **28**, 1156–1167.

Press, W. H., Flannery, B. P., Tekolsky, S. A., and Vetterling, W. T. (1988) *Numerical Recipes in C*, pp. 735. Cambridge University Press, Cambridge.

Pruppacher, H. R. and Klett, J. D. (1978) *Microphysics of Clouds and Precipitation*, pp. 714. D. Reidel, Dordrecht.

Riebesell, U. and Wolf-Gladrow, D. A. (1992) The relationship between physical aggregation of phytoplankton and particle flux: a numerical model. *Deep-Sea Research*, **39**, 1085–1102.

Rodríguez, J. and Li, W. K. W. (1994) The size structure and metabolism of the pelagic ecosystem. *Scientia Marina*, **58**(1–2).

Ruiz, J. (1996) The role of turbulence in the sedimentation loss of pelagic aggregates from the mixed layer. *Journal of Marine Research*, **54**, 385–406.

Ruiz, J. and Izquierdo, A. A simple model for the break-up of marine aggregates by turbulent shear. *Oceanologica Acta* (in press).

Shanks, A. L. and Treut, J. D. (1980) Marine snow: sinking rates and potential role in vertical flux. *Deep-Sea Research*, **27**, 137–143.

Sheldon, R. W., Prakash, A. and Sutcliffe, W. H. (1972) The size distribution of particles in the ocean. *Limnology and Oceanography*, **17**, 327–340.

Smayda, T. J. (1970) The suspension and sinking of phytoplankton in the sea. *Oceanography and Marine Biology: an Annual Review*, **8**, 353–414.

Smith, R. C. and Baker, K. S. (1981) Optical properties of the clearest natural waters. *Applied Optic*, **20**, 177–184.

Stolzenbach, K. D. and Elimelech, M. (1994) The effect of particle density on collisions between sinking particles: implications for particle aggregation in the ocean. *Deep-Sea Research I*, **41**, 469–483.

Tambo, N. and Watanabe, Y. (1979) Physical characteristics of flocs-I. The floc density function and aluminum floc. *Water Research*, **13**, 409–419.

Valiela, I. (1984) *Marine Ecological Processes*, pp. 546. Springer, Berlin.

Wacholder, E. and Sather, N. F. (1974) The hydrodynamic interaction of two unequal spheres moving under gravity through quiescent viscous fluid. *Journal of Fluid Mechanics*, **65**, 417–437.